J Mol Model (2008) 14:559–569
DOI 10.1007/s00894-008-0310-3

ORIGINAL PAPER

The 3D structure of the defense-related rice protein Pir7b predicted by homology modeling and ligand binding studies

Quan Luo · Wei-Wei Han · Yi-Han Zhou · Yuan Yao · Ze-Sheng Li

Received: 11 December 2007 / Accepted: 1 April 2008 / Published online: 1 May 2008

Abstract To better understand the ligand-binding mechanism of protein Pir7b, important part in detoxification of a pathogen-derived compound against *Pyricularia oryzae*, a 3D structure model of protein Pir7b was constructed based on the structure of the template SABP2. Three substrates were docking to this protein, two of them were proved to be active, and some critical residues are identified, which had not been confirmed by the experiments. His87 and Leu17 considered as 'oxyanion hole' contribute to initiating the Ser86 nucleophilic attack. Gln187 and Asp139 can form hydrogen bonds with the anilid group to maintain the active binding orientation with the substrates. The docking model can well interpret the specificity of protein Pir7b towards the anilid moiety of the substrates and provide valuable structure information about the ligand binding to protein Pir7b.

Keywords Defense-related esterase · Homology modeling · Ligand selectivity · Molecular docking · Pir7b

Introduction

Blast disease that causes annual yield loss is one of the three most devastating diseases on rice. Inoculation of leaves with the non-host pathogen *Pseudomonas syringae* pv. *Syringae* will lead to the activation of defense-related genes, which will ultimately induce the systemic resistance to *Pyricularia oryzae*, the causing agent of the rice blast disease [1]. Concomitant with resistance induction, several defense-related gene transcripts simultaneously began to accumulate to high levels. One of the activated genes was cloned and encoded a putative 268 amino-acid protein called Pir7b [2]. It was speculated that protein Pir7b should have a function in pathogen-defense and one possibility would be its involvement in a detoxification process. Protein Pir7b's detoxification capability against a pathogen-derived compound is an interesting and attractive problem to pathologist, and this role has been recently demonstrated for a *p*-nitrophenylbutyrate-hydrolyzing esterase from the bacterium *Pantoea dispersa*, which was reported to detoxify the antibiotic albicidin produced by *Xanthomonas albilineans* [3]. Sequences alignment has shown that Pir7b shares 35% amino acid sequence identity with *Hevea brasiliensis* hydroxynitrile lyase (HNL) and 40% with esterase Salicylic acid-binding protein (SABP2). The catalytic triad Ser86, Asp218 and His246 were conserved in Pir7b sequence [4]. Based on lots of known crystal structures α/β hydrolase, a Ser-His-Asp catalytic triad in the active site could be regarded as a characteristic, as well as the common structural framework of the α/β hydrolase fold, which is made up of a mostly parallel β-sheet, flanked on both sides by α-helices. The nucleophile is usually located in a very sharp turn, called the 'nucleophile elbow', which is identified from the consensus sequence G-x-(nucleophile)-x-G. The geometry of the nucleophile elbow also contributes to the formation of the oxyanion-binding site, which is usually formed by two backbone nitrogen atoms and needed to stabilize the negatively charged transition state that occurs during hydrolysis [5–7].

The experimental results indicated that recombinant Pir7b produced in *E. coli* and yeast tested for enzyme activities could occur within the α/β hydrolase superfamily.

Q. Luo · W.-W. Han · Y.-H. Zhou · Y. Yao · Z.-S. Li (✉)
State Key Laboratory of Theoretical and Computational Chemistry, Institute of Theoretical Chemistry, Jilin University, Changchun 130023, People's Republic of China
e-mail: zeshengli@mail.jlu.edu.cn

Screening from a set of artificial substrates, positive results were obtained in esterase activity tests when 2-naphthol AS-acetate and related compound 2-naphthol AS- 2-chlor-propionate were used as substrates. The anilid moiety of the substrates was thought to be important, as none of the usually well accepted naphthol esters lacking it were hydrolyzed to a detectable level [4]. However, the detailed mechanism of ligand-receptor interactions remains unclear due to the lack of a 3D structure of the Pir7b. In this paper, a 3D model of Pir7b was constructed based on the known structure of template SABP2 and HNL by using homology modeling and refined by molecular dynamics simulations. The refined Pir7b model was used to study the binding mechanism of two active naphthol esters and a related inactive compound. Based on the ligand binding study, a ligand selectivity mechanism is proposed.

Theory and methods

1. Template selection

BLAST search has shown that the sequences identities between protein Pir7b and homologous proteins SABP2 (1Y7I.pdb) and HNL (6YAS.pdb) are 40% and 35%, respectively [8–10]. Due to the biochemical function study protein Pir7b, it belongs to esterase, which preferentially breaks ester bonds of shorter chain fatty acids. Thus, we chose SABP2 as our template protein to construct the target protein [11–13]. In order to confirm that the choice of the template was suitable for the target protein, a detailed examination of the 2D structural feature of protein Pir7b was carried out by using APSSP [14], GOR [15], NNPREDICT [16], SOPMA [17] and HNN [18]. The secondary structure alignment was subsequently performed by using ClustalW Multiple sequence tools [19]. The result that closely resembled secondary composition patterns was easily identified and supported our template selection.

2. Homology modeling of Pir7b structure

The initial structure of Pir7b was built by homology modeling based on the structure of SABP2 by means of MODELLER program, and the conformations of side chains were explored by using rotamers. Since the initial model protein inevitably contained some serious steric overlaps [20], we designed a specific optimization protocol for fully relaxing our initial model while preserving its inherited topological features. The consistent-valence force field (CVFF) was used for all the simulation procedures [21]. The refinement was accomplished in multiple-step including restrained energy minimization and molecular dynamics simulation. First, 100 steps of steepest descent (SD) minimization was carried out to correct most severe stereo conflicts while the coordinates of the backbone Cα atoms of all structurally conserved regions (SCR) residues were fixed during this stage of refinement process to prevent SCR from deforming significantly. The further relaxation was followed by 600 steps of conjugate-gradient (CG) minimization process. Due to the fixed atoms in SCRs hindered this optimization process, the constraint on fixed backbone atoms in SCRs was replaced by tether restraints. After the multiple-step energy minimization, a 500 ps dynamics simulation was performed at 298K to search the steady conformation [20]. The restriction condition was further released, but the six central β strands were considered as core domain for providing a stable scaffold for the active sites in α/β hydrolase superfamily, which still kept the original tether restraint [22, 23]. To account for the solvent effect, 5 Å TIP3P water layer was added to the whole protein. The output conformers were collected at every 5 ps and totally 100 conformers were saved in the archive file. Among the 100 conformers, 10 conformers with low total energy were selected and the priority for choosing a conformer was estimated using PROCHECK [24], PROFILE-3D [25, 26] and PROSA [27].

3. Molecular docking

The structures of 2-naphthol AS-acetate, 2-naphthol AS-2-chlor-propionate and 2-naphthol-acetate were optimized at the B3LYP/6-311G* level to study their possible binding modes to Protein Pir7b [28]; the former two ligands were active, while the latter one was related inactive. We first defined a binding site subset which included important residues suggested by other studies [4]. Then a two-step docking procedure was carried out to dock substrates to protein Pir7b by using a combination of Monte Carlo, simulated annealing and minimization. During the first phase, Monte Carlo minimization approach was fulfilled to obtain reasonably placed ligands, and Quartic-Vdw-no-Coul nonbond method was used for nonbond contacts. We imported the initial structures generated by the first phase Monte Carlo minimization to a more realistic approach, cell-multipole nonbond method, to further refine the docking result. Finally, the docked complexes of protein Pir7b with naphthol esters were selected by the criteria of interaction energy combined with the geometrical matching quality [29–31].

4. Molecular dynamics simulations

The three docked complexes were embedded in a 6Å TIP3P water layer, which was solvated in a truncated octahedral periodic box. Here, Na ions were added to neutralize the negative charge of protein Pir7b. Each enzyme-substrate complex was fixed, and only the positions of waters and ions were minimized. Then the entire simulation system was subjected to energy minimization. The following 20 ps MD simulation was carried out at

constant volume condition, and the temperature was heated up from 0K to 298K at this pressure by using Langevin temperature equilibration scheme, while 1.5 ns dynamics simulation was performed succedently at 298K by using constant pressure condition. All these MD simulation were executed to equilibrate the whole protein Pir7b and naphthol esters complex system [32–34]. The potential energy and the RMS deviations of each Pir7b-substrate complex were monitored to see whether the conformations of the three enzyme-substrate complexes were stable enough or not during MD simulation.

MD simulation was performed with the amber software package, using periodic boundary conditions [35]. A more popular FF99 force field and particle-mesh Ewald (PME) method were used to calculate the electrostatic interactions [36, 37].

Result and discussion

1. Homology modeling of Pir7b

The alignment of two template proteins against the target sequence was used to find the regions where the structures of these proteins were most matched. The matched structures can be taken as the structures of the corresponding regions in the target sequence (Fig. 1). Moreover, the secondary structure of the target sequence was predicted by using several protein secondary structure prediction programs mentioned above, and the predicted results would refine the initial model (Fig. 2). The overall quality of the initial model was examined by PROFILE-3D, and the sum of the self-compatibility score for this model is 90.6 which lies between the score expected for a correct structure (121.8) and the typical value for a grossly misfolded structure (54.8). Shown as the graph of the local compatibility score S (Fig. 3a), four regions, residues 123–132, 138–146, 189–197, 260–268, might be misfolded and required further improvement, which got negative compatibility score, Because the structural errors based on the results from PROFILE-3D hardly occurred at the structurally conserved regions (SCRs), a tether restraint was imposed on the model to preserve all geometric features of SCRs in the following optimization procedure. The final unperturbed conformations of the model protein were acquired by progressively relaxing parts of the initial model. A plot of the total energy versus time of MD simulation was displayed in Fig. 4. 10 conformers with the lowest total energy were selected after the total energy reached the minimum. The most reasonable conformer was determined by using various different evaluation methods as discussed in the following section.

2. Model evaluation

The structure of the refined model was evaluated by programs PROCHECK, PROFILE-3D, and PROSA. As to the assessment of protein Pir7b model by PROCHECK, the reliability backbone torsion angles Φ, φ of the target protein were examined and a percentage quality measurement of a protein structure were used, which had four sorts of occupancies called “core”, “allowed”, “generously allowed” and “disallowed” regions, respectively. The values calculated for Pir7b model and template SABP2 are shown in Table 1. The occupancy rates of core, allowed and generously allowed regions for the predicted structure of protein Pir7b were slighty worse than the values evaluated for the template protein structure (98.7 versus 99%). Only three C-termini residues Arg254, Leu260 and Glu255 in disallowed regions, because the ends of protein are often flexible. PROFILE-3D aligned a sequence with the 3D

Fig. 1 Multiple sequence alignment of Pir7b with SABP2 and HNL. Red boxes show identical residues, yellow boxes show conserved substitutions, and light blue boxes show semi-conserved substitutions

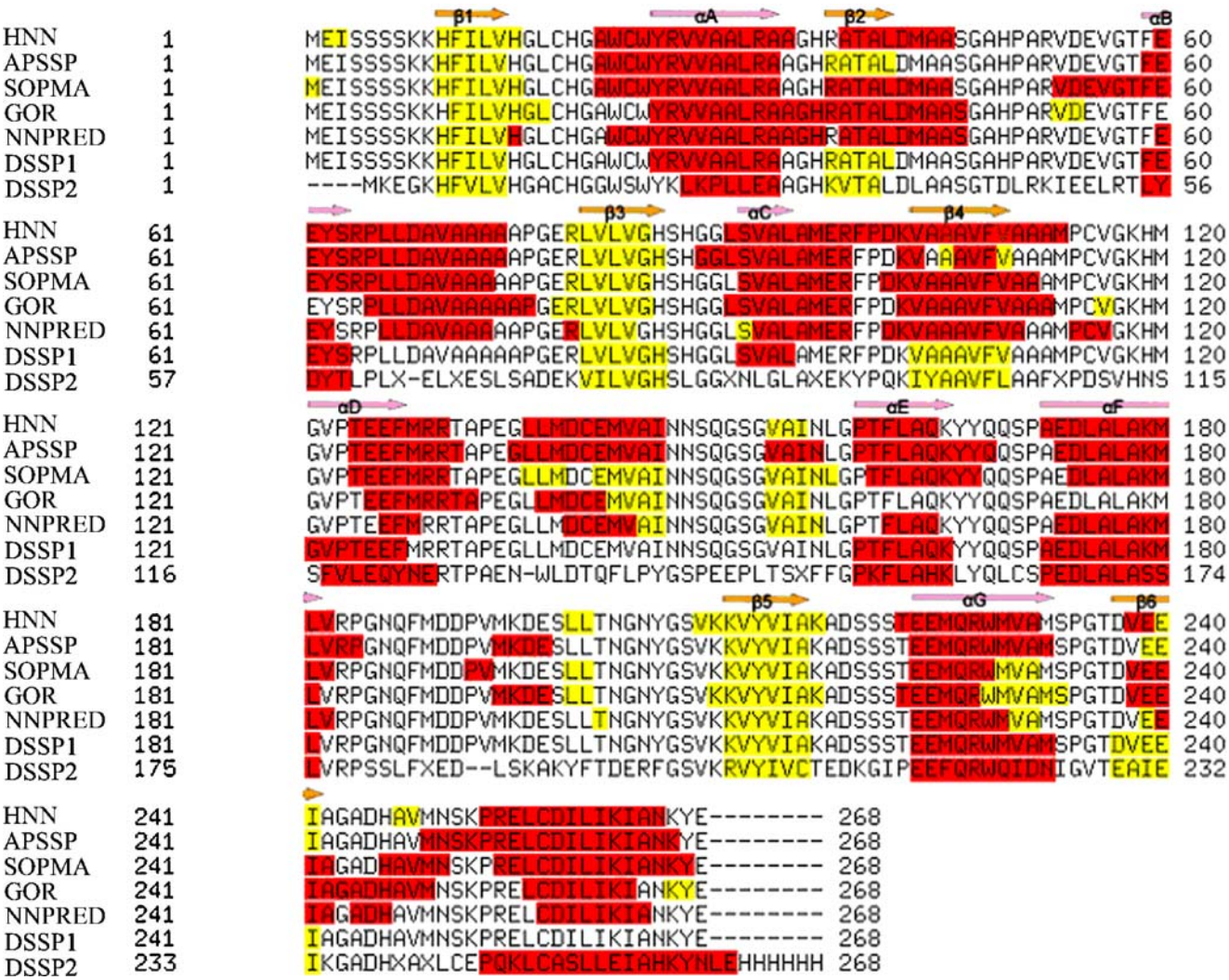

Fig. 2 The secondary structure prediction results of Pir7b sequence using HNN, APSSP, SOPMA, GOR and NNPREDICT. The residues in Red boxes and yellow boxes represent α helix and β strand, respectively. The secondary structures for the refined protein model pir7b2 (DSSP1) and the template structure SABP2 (DSSP2) are defined by the DSSP program and aligned with those predicted

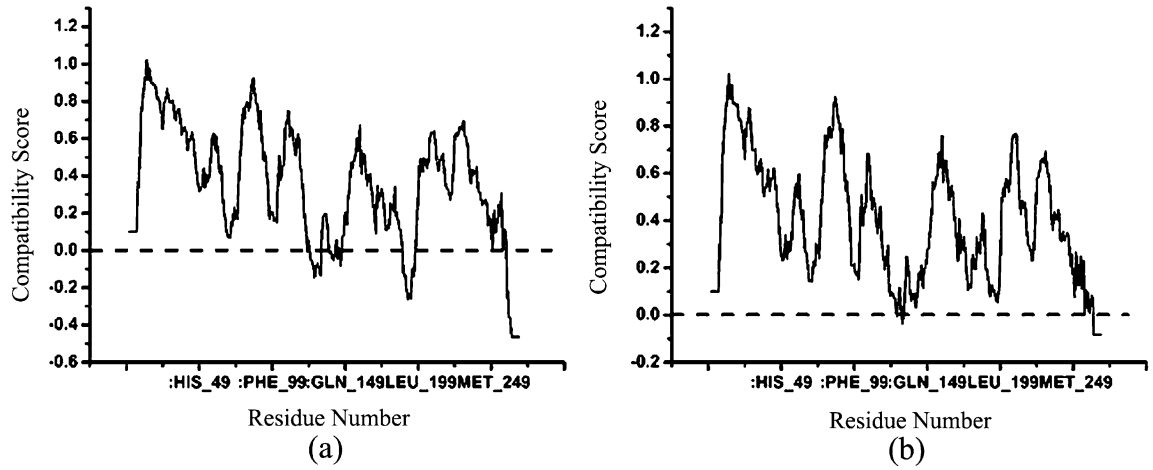

Fig. 3 3D profiles of verified results of the initial protein model pir7b1 (**a**) and the final protein model pir7b2 (**b**). Residues with positive S value are reasonably folded

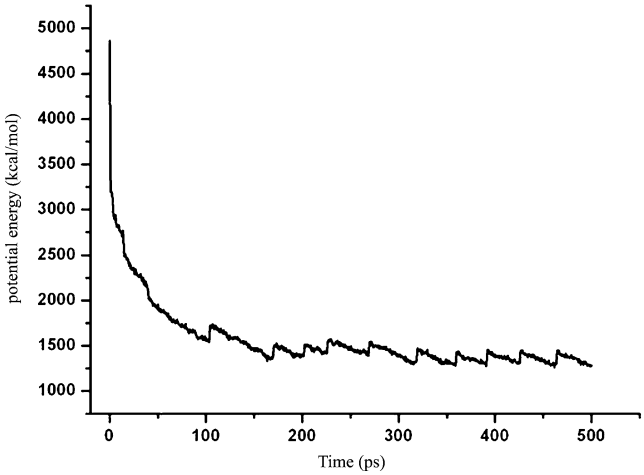

Fig. 4 The variation of potential energy during the 500 ps of MD on the pir7b

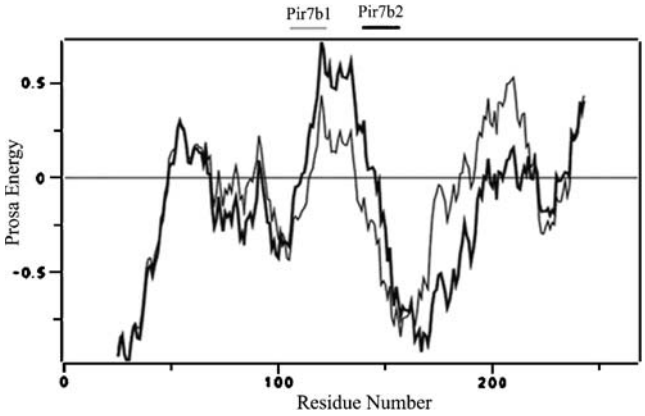

Fig. 5 PROSA energy profile drawn for the initial model (Pir7b1) and MD refined model (Pir7b2) using the PROSA2003 program. Pir7b2 has lower PROSA energy in most structurally conserved regions

profile which is a position-dependent comparison matrix calculated from the probabilities of finding each of the twenty amino acids in each of the environment classes as observed in a database of known structures and related sequences. The resulting alignment score of the final structure was enhanced to 96.9 and the graph of the local compatibility score had been improved, too (Fig. 3b). There were several residues still estimated as false by PROFILE-3D, MET128, ALA132 and ILE263-Glu268. However, all of these regions belonged to variable regions or the ends of protein Pir7b, and all lay on the protein surface, which could not affect the protein folding. A further comparison by the PROSA 2003 program between the initial model (Pir7b1) and MD refined model (Pir7b2) was showed in Fig. 5, which represented the residue interaction energy of the protein. Obviously, the multiple-step optimization procedures did improve in the structure especially for residues in most SCRs because their corresponding PROSA energy was more negative than those energy of the initial structure. With these detailed examination, the final structure of protein Pir7b was accepted for the subsequent binding analysis.

Figure 6a showed a superposition of our Pir7b model with the template protein SABP2. It is clear that the whole topology of the template SABP2 had been inherited while

Table 1 Comparison of theoretical model Pir7b with template SABP2

Value calculated	Pir7b structure	Template SABP2 structure
Core	78.1%	86.0%
Allowed	19.3%	13.0%
Generously allowed	1.3%	0.0%
Disallowed	1.3%	1.0%

*The Φ, φ region percentages were calculated by PROCHECK.

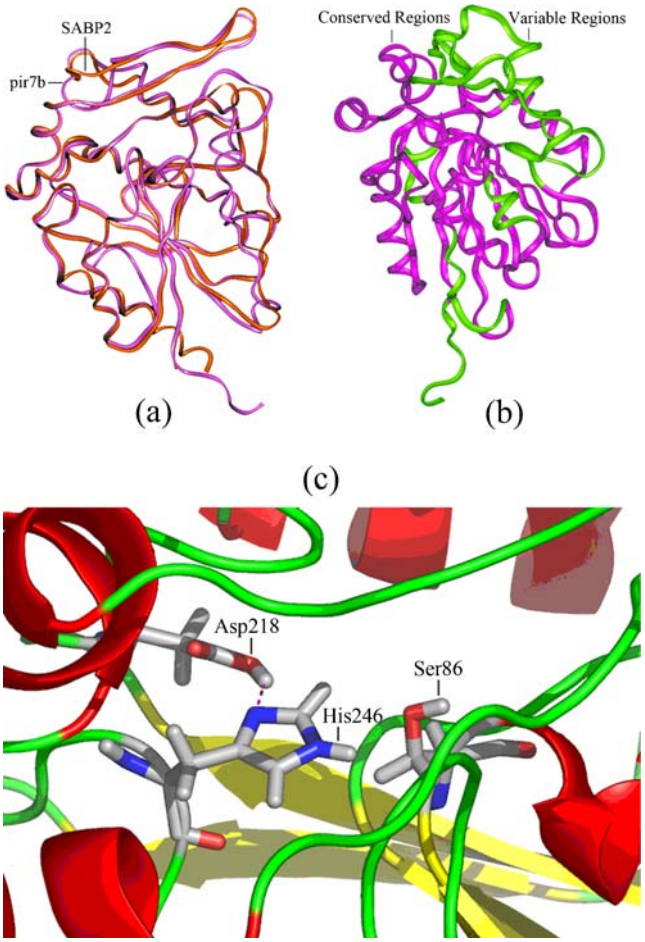

Fig. 6 (**a**) Comparison of refined Pir7b model with its template protein SABP2. Magenta ribbon representation of Pir7b. Orange ribbon representation of SABP2 (**b**) Colored region distribution of Pir7b model. Green, variable regions; magenta, conserved regions. (**c**) The catalytic triad residues of the substrate-free Pir7b model. Hydrogen bond is shown in magenta dash line

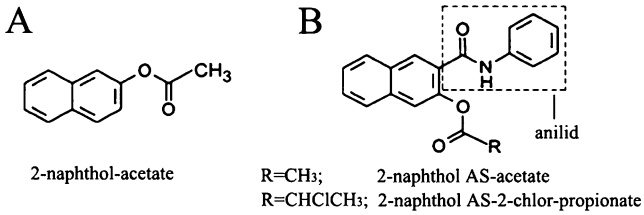

Fig. 7 (**a**) Structure of 2-naphthol-acetate. (**b**) naphthol AS-esters. The anilid moiety of the naphthol AS-esters was thought to be important, as none of the usually well accepted naphthol esters lacking it were hydrolyzed to a detectable level

some changes in local configuration were only presented in variable regions. A multiple-sequence alignment revealed that variable residues 1–8, 67–74, 90–96, 112–156, 189–199, 247–252 were located on the surface of our Pir7b model (Fig. 6b). Based on the structural analysis of the template SABP2, the majority of Residues 112–156 were the cap domain, which allowed the substrate to enter the active site and the product to leave it. Identified by the DSSP program of Kabsch and Sander [38], the core domain contained a central six-stranded parallel β-sheet (named β1–β6) which was flanked on both sides by many helices, and this is in accordance with most results predicted by those secondary structure prediction methods mentioned above (Fig. 2). The catalytic triad of Pir7b, formed by Ser86, His246, and Asp218, was responsible for hydrolysis substrate. Here, Ser86 was suggested to perform a nucleophilic attack on the substrate; His246 acted as a general base in the hydrolytic reaction, abstracting a proton from Asp218. However, in the substrate-free enzyme model, the distance between O atom in Ser-86 and the backbone N atom of His-246 was 3.47 Å. Ser-86 can not be

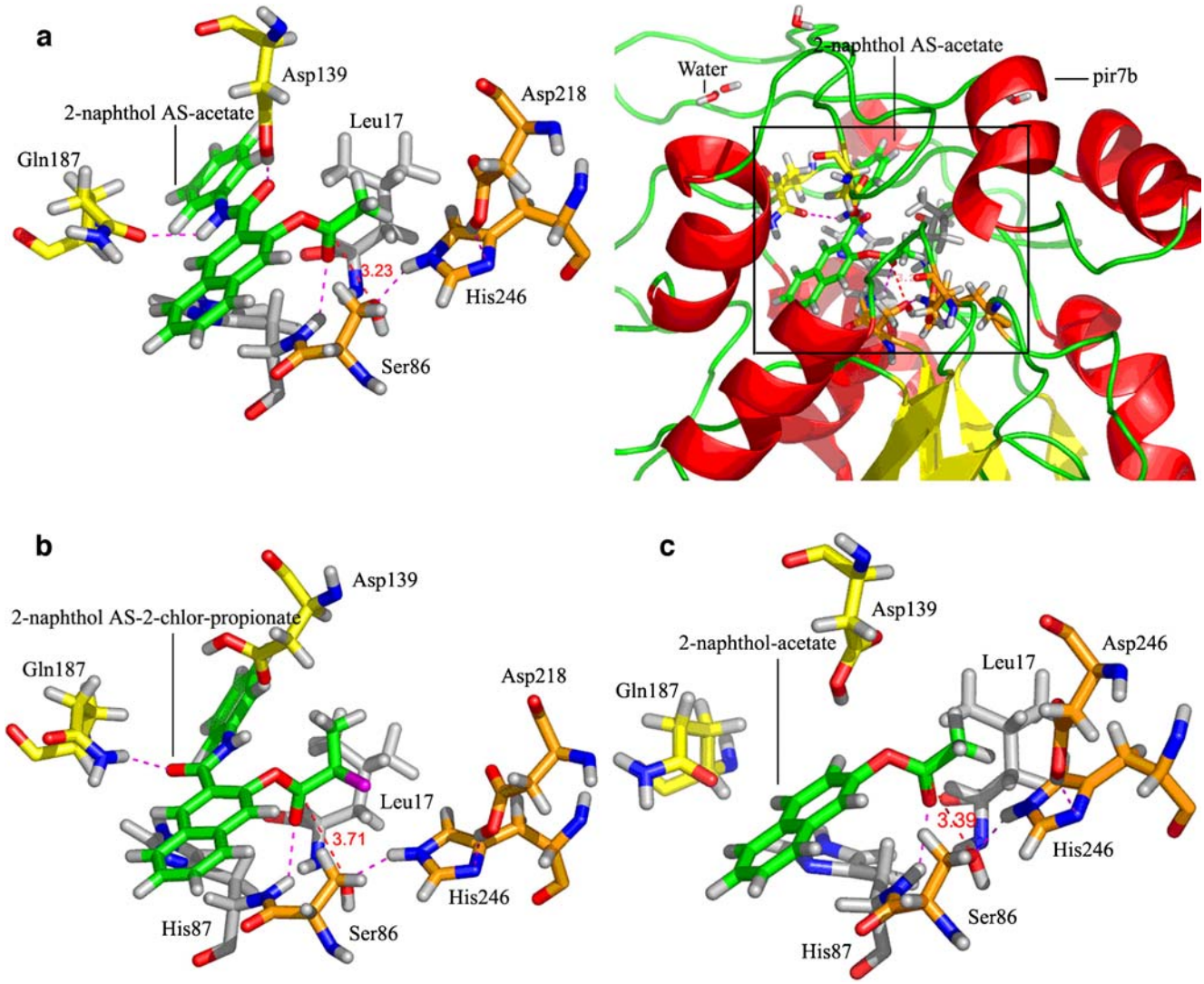

Fig. 8 Ligand binding analysis based on the refined Pir7b model. Magenta dash line, hydrogen bond; Red dash line, distance label. (**a**) Docking of 2-naphthol AS-acetate to Pir7b model. A 3D figure of 2-naphthol AS-acetate-Pir7b complex is also attached (**b**) Docking of 2-naphthol AS-2-chlor-propionate to Pir7b model. (**c**) Docking of 2-naphthol-acetate to Pir7b model

Table 2 Comparison of 2-naphthol AS-acetate-Pir7b complex with 2-naphthol AS-2-chlor-propionate-Pir7b compex about the total energy (E_{total}), van-der-Waals energy (E_{vdw}) and electrostatic energy (E_{ele}) between ligand and individual residues in Pir7b

2-naphthol AS-acetate				2-naphthol AS-2-chlor-propionate		
Residue	E_{vdw} (kcal mol^{-1})	E_{ele} (kcal mol^{-1})	E_{total} (kcal mol^{-1})	E_{vdw} (kcal mol^{-1})	E_{ele} (kcal mol^{-1})	E_{total} (kcal mol^{-1})
Total	−86.60	−18.36	−104.97	−83.25	−13.86	−97.12
His87	−11.94	−3.88	−15.82	−10.64	−2.65	−13.29
Asp139	−1.24	−8.31	−9.55	−3.74	−2.35	−6.09
Gln187	−5.40	−3.44	−8.84	−4.47	−3.47	−7.95
Leu17	−6.67	−2.11	−8.78	−6.58	−0.20	−6.78
Phe127	−5.98	−0.22	−6.20	−5.12	−0.62	−5.74
Glu126	−5.87	0.24	−5.63	−5.88	−0.24	−6.12
Ser86	−5.70	1.21	−4.49	−6.38	1.25	−5.13
Ile155	−3.10	−0.90	−4.00	−2.51	0.09	−2.42

* E_{total}<−4.00kcal mol^{-1} listed in energy rank order

hydrogen-bonded to the second member His-246 residue in the catalytic triad, and the hydrogen-bonding network among the catalytic triad residues was not formed (Fig. 6c).

3. Ligand binding analysis

The refined Pir7b model was used to study its ligand-binding mechanism. Two active ligands 2-naphthol AS-acetate, 2-naphthol AS-2-chlor-propionate and a related inactive compound 2-naphthol-acetate (Fig. 7) were docked into the active-site pocket.

Figure 8a showed the detailed binding mode between 2-naphthol AS-acetate and active site residues in Pir7b model. The hydroxyl of Ser86 can form a hydrogen bond with the N atom of His-246 to complete the catalytic triad. Moreover, the side chain hydroxyl of the catalytic Ser86 was located with a distance of 3.23 Å to the carboxyl carbon of 2-naphthol AS-acetate in a perfect position for initiating the nucleophilic attack. His87, considered as 'oxyanion hole', had a backbone NH group hydrogen bonded to the carboxyl oxygen of substrate, which facilitated the negatively charged transition state more stable, which evolved from the nucleophilic Ser86 during the hydrolysis of the covalent enzyme-substrate intermediate, This is consistent with most solved three-dimensional crystal structures of α/β hydrolase, in which one of 'oxyanion hole' is usually immediately followed by the nucleophile [5]. Gln187 and Asp139 were hydrogen bonded, respectively, to the anilid moiety NH group and carbonyl oxygen of 2-naphthol AS-acetate, their participation in ligand binding were beneficial for a perfect docking orientation by retaining most of favorable interactions and avoiding steric clashes between the ligand and receptor.

To find the other key residues contributed to the high binding affinity of 2-naphthol AS-acetate for protein Pir7b, the interaction energies of this ligand with each of the residues in the active-site pocket were calculated. Table 2 listed the interaction energies including the total energies, van-der-Waals, and the electrostatic energies; the residues which had the total energy lower than —4.0 kcal mol^{-1} were recorded as well. The complex had a large favorable total interaction energy of −104.97 kcal mol^{-1}, the van-der-Waals and electrostatic energies were −86.60 and −18.36 kcal mol^{-1}, respectively. Due to the interaction energy analysis, residues His87, Ile155, Phe127, Leu17 and Glu126 were speculated to share the favorable van-der-Waals interactions with the substrate, and the side chains of these residues can provide a rather hydrophobic environment for the phenyl of 2-naphthol AS-acetate.

Table 3 The distances between the carboxyl O (N) of the substrates and Ser86 (O), His87 (N) and Leu17 (N)

Substrate	Atom1	Residue	Atom2	Distance
2-naphthol AS-acetate	carboxyl (C)	Ser86	hydroxyl (O)	3.23 Å
	carboxyl (O)	His87	backbone (N)	3.24 Å
	carboxyl (O)	Leu17	backbone (N)	3.24 Å
2-naphthol AS-2-chlor-propionate	carboxyl (C)	Ser86	hydroxyl (O)	3.71 Å
	carboxyl (O)	His87	backbone (N)	3.16 Å
	carboxyl (O)	Leu17	backbone (N)	3.34 Å
2-naphthol-acetate	carboxyl (C)	Ser86	hydroxyl (O)	3.39 Å
	carboxyl (O)	His87	backbone (N)	3.26 Å
	carboxyl (O)	Leu17	backbone (N)	3.26 Å

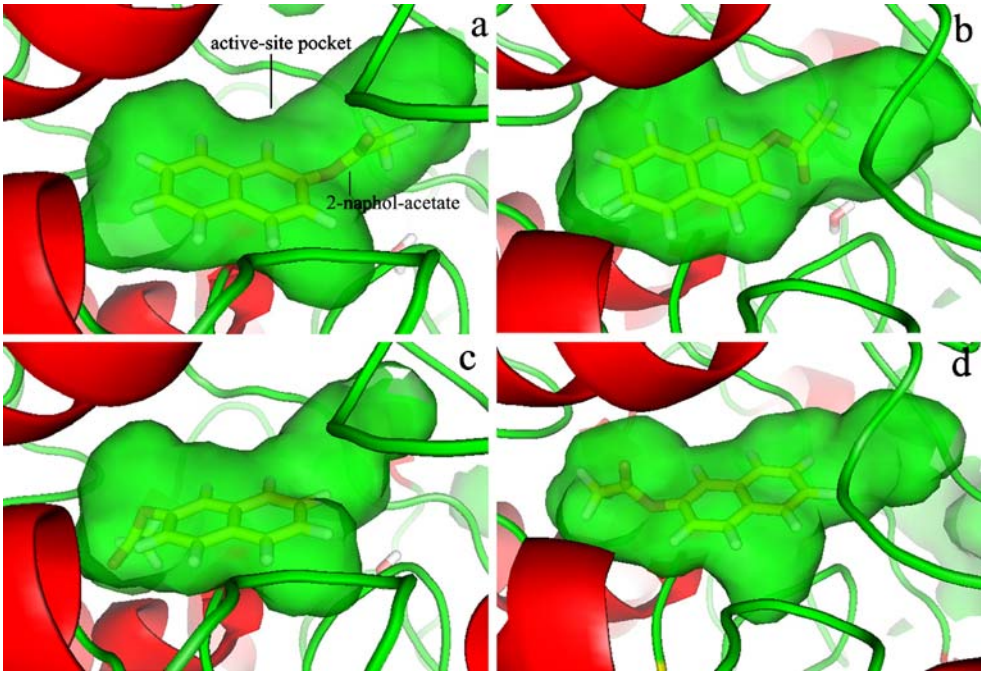

Fig. 9 Four inactive orientations of the 2-naphthol-acetate in active site. The corresponding interaction energies of these binding modes are approximated to the interaction energy of the possible active binding mode

An interesting observation was that the distance from the N atom of Leu17 to the carboxyl oxygen of the ligand was 3.24 Å, which was equal to the distance between the His87 backbone N atom and the carboxyl oxygen of the ligand. By assuming a different torsion angle, the NH group of these residues, Leu17 and His87, can act as a hydrogen-bond donor and bond to the ligand carboxyl oxygen. It can be concluded that the 'oxyanion hole' should be composed by hydrogen bonds from the backbone N atoms in His87 and Leu17.

With regard to the docking of 2-naphthol AS-acetate with the target protain, the binding analysis of another active ligand 2-naphthol AS-2-chlor-propionate with protein Pir7b was performed. A similar binding complex was achieved by superimposing its carboxyl with that of docked 2-naphthol AS-acetate (Fig. 8b). The maximum difference between 2-naphthol AS-2-chlor-propionate-Pir7b complex and 2-naphthol AS-acetate-Pir7b complex is the interaction of Asp139 with the ligand. As a result of the influence of chloroethyl, the anilid moiety of 2-naphthol AS-2-chlor-propionate was turned nearly 180° relative to its position in 2-naphthol AS-acetate-Pir7b complex, and the carboxylic acid group of Asp139 can not form a hydrogen bond with the carbonyl oxygen of the anilid moiety to stabilize the configuration of the substrate any more.

Because the destabilized hydrogen bond between Asp139 and 2-naphthol AS-2-chlor-propionate may affect nucleophilic attack, a detailed distance comparison surrounding the nucleophilic site was made between the two active ligand-Pir7b complexes, presented in Table 3. The distance between the Leu17 backbone N atom and the ligand carboxyl oxygen atom and the distance from the Ser86 hydroxyl oxygen atom to the ligand carboxyl carbon atom in the 2-naphthol AS-2-chlor-propionate-Pir7b complex were both elongated a little relative to the 2-naphthol AS-acetate-Pir7b complex, which were 3.34 Å and 3.71 Å, respectively. This distance changes was not favorable to the Ser86 nucleophilic attack but still within an acceptable range, then it can be concluded that the catalytic activity of Pir7b decreased with the increasing of the fatty acid carbon chains of the ligand. This was in good agreement with that of esterase (HSR 203J) which hydrolyzed p-nitrophenyl acetate and related short-chain acyl esters and had related functions in pathogen defense [4, 39]. Furthermore, the total interaction energy and the interaction energies of the 2-naphthol AS-2-chlor-propionate with each of the residues

Table 4 The total energy (E_{total}), van-der-Waals energy (E_{vdw}) and electrostatic energy (E_{ele}) between 2-naphthol-acetate and individual residues in Pir7b

Residue	E_{vdw} (kcal mol^{-1})	E_{ele} (kcal mol^{-1})	E_{total} (kcal mol^{-1})
total	−55.42	−4.25	−59.67
His87	−7.26	−1.69	−9.95
Glu126	−5.45	−0.13	−5.80
Ser86	−5.51	1.07	−4.44
Leu17	−2.96	−1.21	−4.17
Glu197	−2.95	−0.36	−3.21
phe127	−3.07	0.01	−3.06

*E_{total}<−3.00kcal mol^{-1} listed in energy rank order

Table 5 The interaction energies of the four inactive 2-naphthol-acetate-Pir7b complex conformations

Conformation	E_{vdw} (kcal mol^{-1})	E_{ele} (kcal mol^{-1})	E_{total} (kcal mol^{-1})
a	−53.66	−7.89	−61.55
b	−56.57	−0.51	−57.08
c	−54.47	6.75	−61.22
d	−49.61	−11.57	−61.19

in the active site were obtained to investigate whether 2-naphthol AS-2-chlor-propionate can steadily bind with protein Pir7b or not. Table 2 summarized the total interaction energy of AS-2-chlor-propionate-Pir7b complex which decreased by 7.5% relative to the 2-naphthol AS-acetate-Pir7b complex. The results of binding structure and energy analysis implied that there was no apparent activity loss in 2-naphthol AS-2-chlor-propionate docking.

After the binding analysis of active ligand compounds presented above, a binding study on inactive ligand 2-naphthol-acetate also provided more information about the mechanism of protein Pir7b interacting with its ligands. In this docking study, it is surprising that many kinds of binding modes with similar interaction energy can be found. However, after structural analysis, only one binding mode seemed to be possible active, shown as Fig. 8c. Hydrogen bond between the hydroxyl oxygen of Ser86 and the imidazolyl N atom of His246 was formed to establish the catalytic triad. The substrate in the complex was found to be in a perfect position for nucleophilic attack by Ser86, and the distance from the Ser86 hydroxyl oxygen to the carboxyl carbon of 2-naphthol-acetate was 3.39 Å (Table 3). Hydrogen bond between the backbone N atom of His87 and the carboxyl oxygen of the substrate was 3.26Å, identical with the distance between the N atom of Leu17 and the carboxyl oxygen of the ligand, which means His87 and Leu17 constituted the oxyanion hole as their character in the former two active complexes.

The possible active binding mode (Fig. 8c) showed that 2-naphthol-acetate may be an active ligand. However, a detailed interaction energy analysis found that 2-naphthol-acetate can not accommodate in the active site as stable as 2-naphthol AS-acetate, because the total interaction energy of the 2-naphthol-acetate-Pir7b complex decreased by 43.2% relative to that of the 2-naphthol AS-acetate-Pir7b complex. The interaction energies of 2-naphthol-acetate with each residue in the active site were calculated, and the residues with the interaction energy lower than −3.0 kcal mol^{-1} were listed in Table 4. It was obvious that the interaction energies between 2-naphthol-acetate and the key residues all decreased, which made the catalysis ability of 2-naphthol-acetate sharply decreased. Furthermore, the shape of active-site pocket and 2-naphthol-acetate's lacking of the anilid moiety could be another reason to make this ligand related inactive, because it can move free in the big active-site pocket. As for the other 2-naphthol-acetate-Pir7b binding modes mentioned above, four representative orientations selected among them were shown in Fig. 9, and the corresponding interaction energies were listed in Table 5. All the interaction energies of the four complexes were about −60.00 kcal mol^{-1}, approximately equal to the interaction energy of the possible active binding mode (Fig. 8c), and they were all considered to be inactive based on the structure analysis without any exception. The

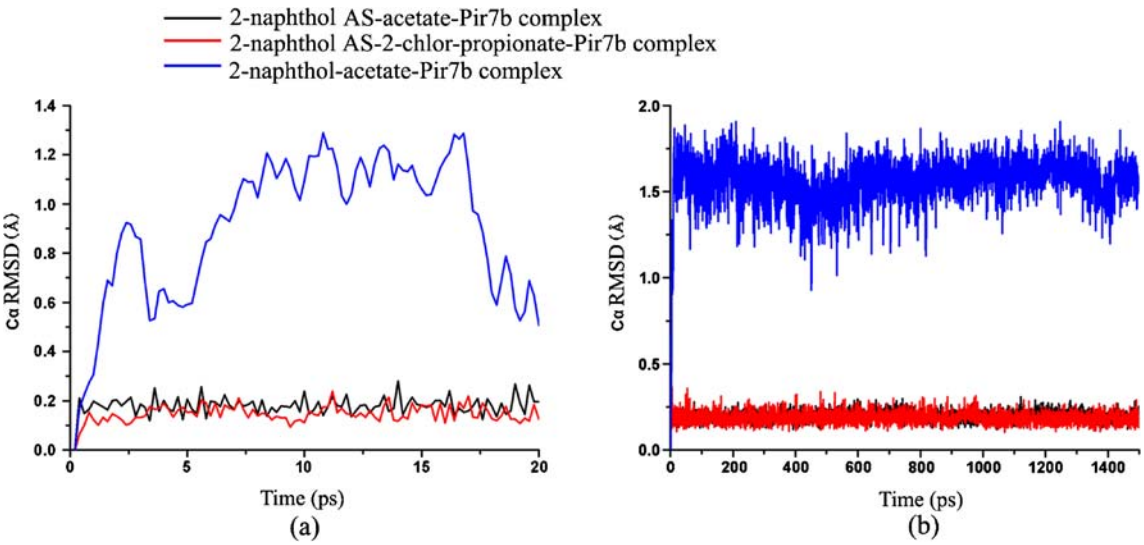

Fig. 10 The RMSD of the Cα of the key residues Asp139, Gln187, Leu17, His87, Ser86, His246, Asp218 and substrates (2-naphthol AS-acetate-Pir7b, 2-naphthol AS-2-chlor-propionate or 2-naphthol-acetate) during 1.7 ns MD simulations. (**a**) 20ps MD simulation at constant volume condition (**b**) 1.5 ns MD simulation at constant pressure condition

reasons were as follows: I) The nucleophilic Ser86 was far from the carboxyl carbon of 2-naphthol-acetate or can not form the catalytic triad; II) Hydrogen bonds can not be formed between the 'oxyanion hole' and the carboxyl oxygen of 2-naphthol-acetate. Considering these inactive binding modes with close interaction energy reduced the chance to form the possible active binding mode, the catalysis ability of 2-naphthol-acetate further decreased.

In order to confirm the stability and reliability of these three docking models, amber9 was used to perform 1.7 ns dynamics simulation to the three possible active binding modes. For all enzyme-substrate complexes, the potential energies are relatively stable during the last 1.5ns MD Equilibration. However, the variations of the RMS deviations of the key residues Asp139, Gln187, Leu17, His87, Ser86, His246, Asp218 and substrates in the three simulation systems indicated that the stability of 2-naphthol-acetate-Pir7b complex was worse than that of the other two complexes; 2-naphthol-acetate had a big-range of swinging in the active pocket during the first 20ps heating MD simulation. Seen from Fig. 10a, the maximal RMSd value of the key residues and substrate in the 2-naphthol-acetate-Pir7b complex came up to 1.3Å, which is almost 6 times higher than the 0.2Å value in the other two complexes. The next 1.5ns equilibrium process (Fig. 10b) showed that 2-naphthol-acetate departed from the possible active binding position abruptly at the beginning, and then returned to a relatively stable stage. The corresponding RMSd value also sharply increased to about 1.7Å and then remained with a fluctuation of 0.5Å. On the other hand, the stability of the other two enzyme-substrate complexes were well retained with a fluctuation of 0.1Å in the RMSd values (Fig. 10b). The results presented here strongly supported the hypothesis that these inactive binding modes of 2-naphthol-acetate-Pir7b would hinder the formation of the possible active binding mode and make the ligand 2-naphthol-acetate to be related inactive.

Finally, a sequence alignment analysis between protein Pir7b and the template SABP2 on the critical residues in the active site illuminated that most key residues except the extremely conserved catalytic triad had altered in Pir7b. Leu82 and Ala13 in SABP2 were replaced by His87 and Leu17 considered as the 'oxyanion hole'. The changed residue Gln187 contributed to the anilid moiety specificity by forming a hydrogen bond with the substrates to maintain the orientation. Asp139, conserved in Pir7b, also seemed reponsible for the binding selectivity; however, the result of docking 2-naphthol AS-2-chlor-propionate suggested that substrate can stably combine with the active site without Asp139. Other shifted residues like Phe127, Ser221, Gln197, Leu157, Asn156 and Ala110 might more or less affect the binding selectivity as well.

As discussed above, it is concluded that protein Pir7b can selectively hydrolyze of 2-naphthol AS-acetate and 2-naphthol AS-2-chlor-propionate, because the anilid moiety of these substrates played an important role in positioning the substrates to a perfect position for nucleophilic attack.

Conclusions

Based on the template SABP2, 3D structural model of protein Pir7b has been constructed and optimized by MD simulation. The refined model agree with most solved three-dimensional crystal structural features of α/β hydrolase and have been analyzed by several evaluation softwares, PROCHECK, PROFILE-3D and PROSA. Furthermore, the model was used to study the possible binding mechanism with 2-naphthol AS-acetate, 2-naphthol AS-2-chlor-propionate and 2-naphthol-acetate. All the expected interactions between the active domain amino acids and the substrates could be described in detail. The complex structure can well interpret the specificity of protein Pir7b towards the anilid moiety of the substrates and provide valuable structure information about the ligand binding to protein Pir7b. Our results will be helpful for further redesigning of Pir7b by site-directed mutagenesis in order to improve or change the catalytic capability.

Acknowledgements This work was supported by the National Science Foundation of China (20333050, 20673044), Doctor Foundation by the Ministry of Education, Foundation for University Key Teacher by the Ministry of Education, Key subject of Science and Technology by the Ministry of Education of China, and Key subject of Science and Technology by Jilin Province.

References

1. Smith JA, Metraux JP (1991) Physiol Mol Plant Pathol 39:451–461
2. Reimmann C, Hofmann C, Mauch F, Dudler R (1995) Physiol Mol Plant Pathol 46:71–81
3. Zhang LH, Birch RG (1997) Appl Microbiol 82:448–454
4. Waspi U, Misteli B, Hasslacher M, Jandrositz A, Kohlwein SD, Schwab H, Dudler R (1998) Eur J Biochem 254:32–37
5. Nardini M, Dijkstra BW (1999) Curr Opin Struct Biol 9:732–737
6. Fojan P, Jonson PH, Petersen MTN, Petersen SB (2000) Biochimie 82:1033–1041
7. Hakulinen N, Tenkanen M, Rouvinen J (2000) J Struct Bio 132:180–190
8. Altschul SF, Madden TL, Schaffer AA, Zhang J, Zhang Z, Miller W, Lipman DJ (1997) Nucleic Acids Res 25:3389–3402
9. Forouhar F, Yang Y, Kumar D, Chen Y, Fridman E, Park SW, Chiang Y, Acton TB, Montelione GT, Pichersky E, Klessig DF, Tong L (2005) Proc Natl Acad Sci USA 102:1773–1778
10. Zuegg J, Gruber K, Gugganig M, Wagner UG, Kratky C (1999) Protein Sci 8:1990–2000

11. Kumar D, Klessig DF (2003) Proc Natl Acad Sci USA 100:16101–16106
12. Klessig DF, Durner J, Noad R, Navarre DA, Wendehenne D, Kumar D, Zhou JM, Shah J, Zhang S, Kachroo P, Trifa Y, Pontier D, Lam E, Silva H (2000) Proc Natl Acad Sci USA 97:8849–8855
13. Gruber K, Gartler G, Krammer B, Schwab H, Kratky C (2004) J Biol Chem 279:20501–20510
14. Raghava GPS (2000) CASP 4:75–76
15. Garnier J, Osguthorpe DJ, Robson B (1978) J Mol Biol 120:97–120
16. Zhang CT, Zhang R (2000) J Biomol Struct Dyn 17:829–842
17. Geourjon C, Deleage G (1995) Comput Appl Biosci 11:681–684
18. Han CL, Zhang W, Dong HT, Han X, Wang MJ (2006) Interferon Cytokine Res 26:441–448
19. Higgins DG, Bleasby AJ, Fuchs R (1992) Comput Appl Biosci 8:189–191
20. InsightII, Homology User Guide, SanDiego:Biosym/MSI (2000)
21. Hakulinen N, Tenkanen M, Rouvinen J (2000) J Struct Biol 132:180–190
22. Ke YY, Chen YC, Lin TH (2006) J Comput Chem 27:1556–1570
23. Yang H, Ahn JH, Ibrahim RK, Lee S, Lim Y (2004) J Mol Graph Model 23:77–87
24. Laskowski RA, Moss DS, Thornton JM (1993) J Mol Biol 231:1049–1067
25. Insight II Profiles-3D, MolecularSimulations Inc, San Diego (2000)
26. Luthy R, Bowie JU, Eisenberg D (1992) Nature 356:83–85
27. Sippl MJ (1993) J Comput Aided Mol Des 7:473–501
28. Frisch MJ, Trucks GW, Schlegel HB Gaussian 03 (Revision A.1) Gaussian Pittsburgh (2003)
29. Affinity San Diego Molecular Simulations Inc (2000)
30. Bartlett P A, Shea G.T, Telfer SJ, Waterman S (1989) R Soc Chem 182–196
31. Shoichet BK, Kuntz ID, Bodian DL (1992) J Comput. Chem 13:380–397
32. Harvey SC, McCammon JA (1987) Cambridge University Press
33. Simmerling C, Strockbine B, Roitberg AE (2002) J Am Chem Soc 124:11258–11259
34. Hornak V, Okur A, Rizzo R, Simmerling C (2006) Proc Nat Acad Sci USA 103:915–920
35. Case DA, Cheatham TE, Darden T, Gohlke H, Luo R, Merz KM, Onufriev A, Simmerling C, Wang B, Woods RJ (2005) J Comput Chem 26:1668–1688
36. Ponder JW, Case DA (2003) Adv Prot Chem 66:27–85
37. Pratt LR, Hummer G., Melville Ed (1999) American Institute of Physics, Melville, New York pp. 104–113
38. Kabsch W, Sander C (1983) Biopolymers 22:2577–2637
39. Baudouin E, Charpenteau M, Roby D, Marco Y, Ranjeva R, Ranty B (1997) Eur J Biochem 248:700–706